Structure, Topology, and Tilt of Cell-Signaling Peptides Containing Nuclear Localization Sequences in Membrane Bilayers Determined by Solid-State NMR and Molecular Dynamics Simulation Studies†

Ayyalusamy Ramamoorthy,*,‡,§ Senthil K. Kandasamy,|| Dong-Kuk Lee,‡,§,⊥ Srikanth Kidambi,‡ and Ronald G. Larson||

Biophysics Research Division, Department of Chemistry, and Department of Chemical Engineering, University of Michigan, Ann Arbor, Michigan 48109-1055

Received September 12, 2006; Revised Manuscript Received November 17, 2006

ABSTRACT: Cell-signaling peptides have been extensively used to transport functional molecules across the plasma membrane into living cells. These peptides consist of a hydrophobic sequence and a cationic nuclear localization sequence (NLS). It has been assumed that the hydrophobic region penetrates the hydrophobic lipid bilayer and delivers the NLS inside the cell. To better understand the transport mechanism of these peptides, in this study, we investigated the structure, orientation, tilt of the peptide relative to the bilayer normal, and the membrane interaction of two cell-signaling peptides, SA and SKP. Results from CD and solid-state NMR experiments combined with molecular dynamics simulations suggest that the hydrophobic region is helical and has a transmembrane orientation with the helical axis tilted away from the bilayer normal. The influence of the hydrophobic mismatch, between the hydrophobic length of the peptide and the hydrophobic thickness of the bilayer, on the tilt angle of the peptides was investigated using thicker POPC and thinner DMPC bilayers. NMR experiments showed that the hydrophobic domain of each peptide has a tilt angle of 15 ± 3° in POPC, whereas in DMPC, 25 ± 3° and 30 ± 3° tilts were observed for SA and SKP peptides, respectively. These results are in good agreement with molecular dynamics simulations, which predict a tilt angle of 13.3° (SA in POPC), 16.4° (SKP in POPC), 22.3° (SA in DMPC), and 31.7° (SKP in DMPC). These results and simulations on the hydrophobic fragment of SA or SKP suggest that the tilt of helices increases with a decrease in bilayer thickness without changing the phase, order, and structure of the lipid bilayers.

The noninvasive delivery of peptides, proteins, oligonucleotides, and other functional cargo molecules into living cells is highly dependent on their efficient transport across the plasma membrane barrier (*1*−*7*). Hydrophobic peptides have been successfully used to transport nuclear localization sequences (NLSs[1]) in order to probe intracellular signaling, which involved interactions of thousands of proteins expressed in living cells (*3*, *6*). For example, the cellular import of peptides has been used in the agonist-induced translocation of transcription factor NF-kB, FGF-1-stimulated mitogenesis, the function of an intracellular signaling protein SHc whose overexpression leads to cell transformation in NIH 3T3 fibroblasts, and epidermal growth factor (EGF)-stimulated Ras activation in intact cells (*1*−*7*). Cellular import is also involved in the regulation of intracellular pathways associated with adhesion, signaling, and trafficking to the nucleus. Recent studies have suggested that in general, cell-signaling peptides translocate a functional nuclear localization sequence directly across the plasma membrane bilayers without this sequence interacting with a receptor or transporter protein in the process (*5*, *8*−*10*). However, there are no high-resolution studies on the secondary structure, folding, and membrane interaction of cell-signaling peptides to understand their transport mechanism. In this study, we have, therefore, investigated the structure and topology of two such peptides, SKP and SA (Figure 1), using solid-state NMR experiments and molecular dynamics simulations of lipid bilayers with varying compositions.

Cell-signaling peptides SKP (*6*) and SA (*8*, *9*) each contain a 16-residue hydrophobic sequence in their N-terminus and different types of nuclear localization sequences at the C-terminus. The hydrophobic region is selected from a signaling peptide sequence. The SKP peptide contains a 25-residue nuclear localization sequence of NF-kB p50 and has been shown to inhibit, in a concentration-dependent manner,

† This research was supported by National Institutes of Health Grant AI054515.

* Corresponding author. Phone: (734) 647-6572. Fax: (734) 763-2307. E-mail: ramamoor@umich.edu.

‡ Biophysics Research Division.

§ Department of Chemistry.

|| Chemical Engineering.

⊥ Present address: Seoul National University of Technology, Department of Fine Chemistry, Seoul, Korea.

[1] Abbreviations: CD, circular dichroism; CP, cross polarization; CSA, chemical shift anisotropy; DMPC, 1,2-dimyristoyl- *sn*-glycero-3-phosphatidylcholine; EGF, epidermal growth factor; MAS, magic angle spinning; MD, molecular dynamics; MLVs, multilamellar vesicles; NLS, nuclear localization sequence; NMR, nuclear magnetic resonance; PISA, polarity index slant angle; PISEMA, polarization inversion spin exchange at the magic angle; POPC, 1-palmitoyl-2-oleoyl-*sn*-glycero-3-phosphatidylcholine; PBS, phosphate buffered saline; PME, particle mesh Ewald; REDOR, rotational echo double resonance; RF, radio frequency; SUV, small unilamellar vesicle; TM, tansmembrane; TPPM, two-phase pulse-modulation; Tris, tris hydroxymethylaminoethane.

10.1021/bi061895g CCC: $37.00
Published on Web 01/06/2007

SA: AAVALLPAVLLALLAPAAANYKKPKL

SKP: AAVALLPAVLLALLAPEILLPNNYNAYESYKYPGMFIALSK

TM: AAVALLPAVLLALLA

FIGURE 1: Primary sequence for 26-residue SA, 41-residue SKP, and the transmembrane fragment (TM) peptides. The underlined residues are hydrophobic and identical in all peptides.

the nuclear translocation of NF-kB in cultured endothelial and monocytic cells stimulated with lipopolysaccharide or tumor necrosis factor-alpha (*6*). In the SA peptide, the 16-residue hydrophobic and 7-residue NLSs are connected by a spacer region of three Ala residues. This peptide has been shown to stimulate DNA synthesis in NIH 3T3 cells in an FGF-receptor-independent manner and to induce DNA synthesis in bovine hamster kidney-21 cells (*8*, *9*). Studies have shown that these peptides are not cytotoxic, and deletion of the hydrophobic domain or mutation of the NLS abolishes the activity of the peptide (*6*, *8*−*10*).

Because the above-mentioned functions of these peptides are highly dependent on their ability to interact with cell membranes, structural studies of these peptides could provide insights into their transport mechanism and efficiency of transport across cell membranes. In spite of recent successes in this field, structure determination of membrane-associated peptides and proteins still remains a big challenge. Recently, it has been demonstrated that solid-state NMR studies can address biological questions related to membrane-bound peptides (*11*−*17*) and also determine the backbone conformation (*18*−*27*) and tertiary folding of peptides and proteins in lipid bilayers (*28*−*33*). Most importantly, solid-state NMR experiments can determine the orientation of these molecules in lipid bilayers, which helps in understanding the function of these systems. A complementary approach is to use molecular dynamics (MD) simulations, which are increasingly used to understand the partitioning of peptides in bilayers (*34*−*36*).

In this article, we present results from a combination of solid-state NMR experiments and molecular dynamics simulations. REDOR (rotational echo double resonance) (*37*) experiments on multilamellar vesicles (MLVs) under magic angle spinning (MAS) conditions were used to determine the backbone conformation of SKP and SA peptides, whereas static PISEMA (polarization inversion spin exchange at the magic angle) (*38*−*40*) experiments on mechanically aligned bilayers allowed the measurement of the orientation of the peptide in bilayers. Molecular dynamics simulations were performed on lipid bilayers containing SKP or SA peptides. From the simulations, properties such as peptide secondary structure, peptide tilt angle, and peptide-induced lipid perturbations were calculated. Computational and experimental results are in excellent agreement. Our results suggest that the hydrophobic region of these peptides is helical with a kink caused by the Pro residue. The transmembrane orientation of the hydrophobic helix was found to depend on the hydrophobic mismatch between the hydrophobic thickness of the lipid bilayer and the hydrophobic length of the peptide. However, the backbone conformation of SKP and SA peptides was independent of bilayer composition.

MATERIALS AND METHODS

Materials. DMPC (1,2-dimyristoyl-phosphatidylcholine) and POPC (1-palmitoyl-2-oleoyl-phosphatidylcholine) were purchased from Avanti Polar Lipids (Alabaster, AL). Chloroform and methanol were procured from Aldrich Chemical, Inc. (Milwaukee, WI). Naphthalene was purchased from Fisher Scientific (Pittsburgh, PA). Peptides were synthesized, and cleavage reagents were purchased from Applied Biosystems (Foster City, CA) and Aldrich (Milwaukee, WI). Fmoc-protected amino acids were obtained from Advanced ChemTech (Louisville, KY) and isotopically labeled Fmoc amino acids from Cambridge Isotope Labs (Cambridge, MA). All chemicals were used without further purification. ^{15}N- and ^{13}C-labeled peptides were synthesized and purified at the University of Michigan as explained elsewhere (*6*, *8*, *9*).

Circular Dichroism. SUVs (small unilamellar vesicles) were prepared by suspending dry lipids in Tris buffer (10 mM TrisHCl, 100 mM NaCl, 0.1 mM EDTA at pH 7.4) and sonicating the dispersion until a clear solution was obtained. Peptide stock solutions (100 mM) were also prepared using the Tris buffer. Each sample was prepared as a 1:1 (vol/vol) mixture of peptide and lipid SUV stock solution with additional Tris buffer as needed in a 5 mm quartz cuvette. The sample was then equilibrated to 25 °C in the CD spectrometer (AVIV, Lakewood, NJ) for 20 min, and 8 scans were acquired and averaged. The scan rate was 1 nm/min over the range of 190−280 nm. Background contributions from the buffer and SUVs were removed by subtracting the spectrum of a similar sample without the peptide.

Solid-State NMR. Mechanically aligned bilayers were prepared using the procedure described by Hallock et al. (*41*). Briefly, 50 mg of lipids and an appropriate concentration of peptide were dissolved in a $CHCl_3/CH_3OH$ (2:1) mixture. The sample was dried under a stream of nitrogen and redissolved in the $CHCl_3/CH_3OH$ (2:1) mixture containing equimolar quantities of naphthalene. An aliquot of the solution (∼300 mL) was spread on thin glass plates (11 mm × 22 mm × 50 mm, Paul Marienfeld GmbH and Co., Bad Mergentheim, Germany); 5 to 10 glass plates were used for each sample. The samples were then air-dried and kept under vacuum at 35 °C for at least 24 h to remove naphthalene and any residual organic solvents. After drying, the samples were hydrated at 98% relative humidity using saturated $NH_4H_2PO_4$ solution (*42*) for 1−2 days at 37 °C, after which approximately 4 μL of H_2O was added to the surface of the lipid−peptide film to fully hydrate the samples. The glass plates were stacked, wrapped with Parafilm, sealed in plastic bags (Plastic Bagmart, Marietta, GA), and then kept at 4 °C for about 12 h.

Multilamellar vesicles were prepared by mixing the required amounts of lipids and peptides in 2:1 chloroform/methanol. The solution was first dried under N_2 gas and then under vacuum overnight to completely remove any residual organic solvents. The mixture was resuspended in 60 wt % water by heating in a water bath at 42 °C. The samples were vortexed for 5 min and freeze−thawed using liquid nitrogen several times to obtain a uniform mixture of lipids and peptides.

All of the experiments were performed on a Chemagnetics/Varian Infinity 400 MHz solid-state NMR spectrometer operating at resonance frequencies of 400.138, 161.979,

100.8, and 40.55 MHz for ^{1}H, ^{31}P, ^{13}C, and ^{15}N nuclei, respectively. A Chemagnetics/Varian temperature controller unit was used to maintain the sample temperature, and each sample was equilibrated for at least 45 min before starting the experiment. A home-built double resonance probe, which has a four-turn square-coil (12 mm × 12 mm × 4 mm) constructed using a 2 mm wide flat wire and a spacing of 1 mm between turns, was used for ^{31}P and ^{15}N experiments on aligned samples and a 5 mm double-resonance MAS probe was used for experiments on MLVs under static conditions. In the case of aligned samples, the lipid bilayers were positioned with the bilayer normal parallel to the external magnetic field of the NMR spectrometer. The ^{15}N chemical shift spectrum of a labeled peptide in oriented bilayers was acquired using a cross-polarization (CP) (*43*) sequence with a ^{1}H $\pi/2$ pulse length of 5 μs, 75 kHz CP RF (radio frequency) power, and a 95 kHz two-phase pulse-modulation (TPPM) (*44*) decoupling of protons during acquisition. A 1 ms ramp-CP (*45*) with a 10 kHz ramp on the ^{1}H channel and a recycle delay of 3 s were used. A ramped spin-lock pulse provided a better signal-to-noise ratio than a constant amplitude spin-lock pulse in the proton channel. A typical ^{31}P 90°-pulse length of 3.5 μs was used. ^{31}P chemical shift spectra were obtained using a spin echo sequence (90°-τ-180°-τ-acquired with $\tau = 90$ μs), 65 kHz RF field for TPPM decoupling of protons, and a recycle delay of 3 s. A typical spectrum required the co-addition of about 100 scans for aligned samples and about 1000 transients for MLVs. The ^{31}P chemical shift spectra are referenced relative to 85% H_3PO_4 (0 ppm) (*41*).

2D PISEMA experiments were performed on mechanically aligned lipid bilayers containing a ^{15}N-labeled peptide as mentioned in our previous publication (*40*). A 50 kHz RF field was used in the ^{1}H channel at on-resonance during the preparation 90° pulse and CP, and a 35.355 kHz offset during the Lee−Goldburg (*46*) sequence in the SEMA (spin exchange at the magic angle) (*39*, *40*) sequence (or the t_1 period). RF field strengths of 50 and 61.2 kHz were used to spin-lock the ^{15}N magnetization during ramp-CP (*45*) and SEMA (*39*), respectively. A 81 kHz RF field was used to decouple protons using the TPPM (*44*) sequence during signal acquisition. Because of the low signal-to-noise ratio from bilayer samples, the experimental conditions were first optimized on a single crystal of *n*-acetyl-L-^{15}N-valyl-L-^{15}N-leucine. The optimized experimental conditions were further optimized on a mechanically aligned POPC bilayer containing the SA peptide by carrying out several 1D experiments using the regular PISEMA sequence but for different t_1 time intervals (*39*, *40*). Because the use of a high RF power in the PISEMA experiment could dehydrate the bilayer sample, cold air was circulated in the probe to reduce the effect of RF heat on the sample. In addition, the quality of aligned samples was examined using 1D ^{31}P experiments before and after PISEMA experiments. Data processing was accomplished using Spinsight software (Varian) on a Sun Sparc workstation.

Magic Angle Spinning Solid-State NMR Experiments. A REDOR (*37*) experiment was used to measure isotropic ^{13}C chemical shifts from peptides selectively labeled with ^{13}C and ^{15}N isotopes. REDOR-filtered experiments as described in the literature (*47*) were utilized to suppress the ^{13}C background signal from the lipids of MLVs. A 5 mm triple-resonance Varian/Chemagnetics MAS probe was used, and the sample was spun at a speed of 8 kHz at −20 °C. A 1.0 ms ramp-CP[45] was followed by a REDOR dephasing period and then direct ^{13}C detection under proton decoupling with a recycle delay of 3.8 s. A single 55 kHz ^{13}C refocusing 180° pulse was placed at the center of the REDOR dephasing time; and 88 kHz TPPM[44] decoupling was applied on the proton channel during both dephasing and detection. The ^{15}N and ^{13}C transmitters were set at 115 ppm (relative to liquid ammonia at 25 °C) and 175 ppm (relative to tetramethylsilane), respectively. For the S_1 (that is with 180° pulses in the ^{15}N channel) acquisition, a 45 kHz ^{15}N 180° pulse at the middle and end of each rotor period in the dephasing time was applied. Other details of the REDOR filtering experiment can be found elsewhere (*47*).

Molecular Dynamics Simulations. We performed molecular dynamics simulations on three different sequences (Figure 1) of signaling peptides (SA, SKP, and the presumed transmembrane domain, TM, of SA, and SKP peptides) embedded in POPC and DMPC bilayers. In all peptides, the presumed transmembrane domain is between residues 1 and 16. We used the GROMACS simulation tool (*48*), using the GROMOS96 43a2 force field for the protein and an OPLS based force field for the lipids (*49*). The SPC water model was used. First, ideal helical structures of all three peptides were created using the software SWISSPDB (*50*). Then, a kink of ∼90° was introduced between residues 16 and 17 of the SA and SKP peptides by changing the appropriate torsion angles. This yielded a transmembrane domain roughly perpendicular to the non-transmembrane domain for both SA and SKP peptides. Each of the three peptides was then solvated in a bath of water, and the presumed transmembrane segment of each (residues 1−16) was positionally restrained while a 10 ns simulation was performed in an NPT (constant number of atoms, pressure and temperature) ensemble to relax the side chains and the non-transmembrane residues. Short-range interactions used a cutoff of 1.2 nm, and the PME algorithm (*51*) was used for long-range electrostatic interactions. The temperature was coupled to a Berendsen thermostat at 310 K, with the peptide and water molecules coupled separately with coupling constants of 0.1 ps. The pressure was coupled isotropically to a Berendsen barostat at 1 atm pressure with a coupling constant of 5 ps. The peptide conformation at the end of these simulations was used to perform bilayer simulations.

The initial coordinates of the hydrated POPC and DMPC bilayers were originally obtained from http://moose.bio.ucalgary.ca/files but were subsequently modified to give a sufficient number of water molecules. Each bilayer consisted of 128 lipid molecules (64 lipids per leaflet). After modifications and sufficiently long equilibration runs, the DMPC bilayer had ∼3500 water molecules and the POPC bilayer had ∼5000 water molecules. Each peptide was inserted into the two bilayers using the "hole" protocol (*52*), giving us six different simulation systems. The peptides were inserted such that the presumed transmembrane segment was oriented parallel to the bilayer normal and the Ala-8 residue was in the middle of the bilayer. After insertion, the peptide backbone residues were positionally restrained, and a 5 ns simulation was performed. The simulation conditions were identical to those in the solvated simulations mentioned above, except that a semi-isotropic pressure coupling was

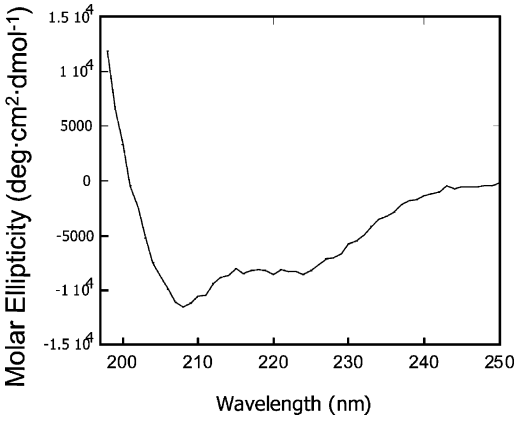

FIGURE 2: CD spectrum of SKP peptide in POPC small unilamellar vesicles at 24 °C.

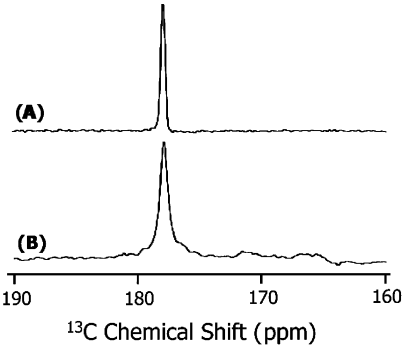

FIGURE 3: REDOR difference ^{13}C chemical shift spectra of POPC multilamellar vesicles containing 3 mol % of (A) SA and (B) SKP peptides. Both peptides contain ^{13}Carbonyl-labeled Leu_{11} and ^{15}N-labeled Leu_{12}. About 20,000 scans were used to obtain the spectra. Other experimental details are given in the text.

used with the normal and lateral directions of the bilayer independently coupled to a pressure bath. After 5 ns, the restraints on the backbone were released, and all six simulations were run for 50 ns. Two simulations (TM peptide in DMPC and POPC) were extended to 100 ns. The coordinates were saved every picosecond and were used in subsequent analyses.

RESULTS

Secondary Structure of SKP and SA Peptides

CD Experiments. The amino acid sequences of SA, SKP, and the hydrophobic segment (noted as TM) peptides are given in Figure 1. CD experiments were performed on SUVs and SDS micelles containing SA and SKP peptides. The concentration of peptides (up to 3 mol %), pH (4 to 7), and lipid composition were varied. SUVs were prepared using DMPC or POPC lipids. The CD spectra of all of these model membrane samples were similar and characterized by the double minima at 208 and 222 nm, attributable to a helical conformation. A representative CD spectrum of SKP in POPC SUVs at 24°C is given in Figure 2. All peptides were assumed to be completely bound to the lipid vesicles at the lipid−peptide ratio of 100:2 used in the present study because the spectra do not change upon increasing the lipid−peptide ratio. The mean helix contents of vesicle-bound SKP and SA, as calculated from the mean residue ellipticity values at l_{222} nm, are about 45% and 60%, respectively.

Magic Angle Spinning NMR Experiments. CD experiments suggest that SKP and SA peptides exist in a helical conformation in membranes. In addition, the dispersion of resonances in 2D ^1H-^1H NOESY spectra of DPC detergent micelles suggest that these peptides form helices (data not shown); samples were prepared by dissolving a lyophilized peptide in an aqueous solution (90% H_2O and 10% D_2O) containing 200 mM perdeuterated DPC (Cambridge Isotope Laboratory) and 20 mM phosphate buffer at pH ~5 at a final concentration of 3 mM. However, determining the conformation of the hydrophobic region of the peptides in lipid bilayers would be useful in understanding the folding of the peptide in membranes. Therefore, we performed MAS experiments on both peptides reconstituted in lipid bilayers. Multilamellar vesicles containing synthetic peptides selectively labeled with ^{13}C and ^{15}N isotopes were used to measure the isotropic ^{13}C chemical shift frequency by performing REDOR experiments (*37*, *53*). Figure 3 shows the difference between the spectra obtained without (S_0) and with (S_1) 180° pulses in the ^{15}N channel. Both experiments were performed with the same number of scans and a 1.6 ms REDOR dephasing time. The spectra of peptides reconstituted in POPC and DMPC MLVs were similar, and therefore, only the spectra obtained from POPC are given in Figure 3. The presence of a single peak with a chemical shift frequency of 177.5 ppm (relative to TMS at 0 ppm) suggests that the ^{13}C-labeled residues are in an α-helical conformation (*54*, *55*). The narrowness of the spectral lines suggests that the peptides are in a single conformation, whereas the observed line width (about 0.5 ppm for SA and 1.5 ppm for SKP peptides) may be attributed to librational motions and/or a small variation in the conformation of the peptides. Although more experimental data are needed to solve the high-resolution structure of the peptide in bilayers, these REDOR data show that the hydrophobic domains (residues 1−14) of both peptides form a helical conformation in lipid membranes. These results are in good agreement with the CD data.

Molecular Dynamics Simulations. All six simulations showed that the transmembrane segment of all of the peptides remains largely helical over the 50-ns duration of the simulation. The secondary structure profiles as a functions of time for TM, SA, and SKP peptides are shown in Figure 4. For the TM peptide, at the beginning of the simulation, residues 2−14 are α-helical (blue). This segment remains helical, for almost the entire duration of the simulation, except for the last 15 ns, when slight fraying is observed at the N-terminal. For the SA peptide, as the simulation progresses, the N-terminal region of the transmembrane domain (residues 1−4) and the non-transmembrane region (residues 17−26) both lose their helicity, leading to other motifs, such as bend, turn, and coil. However, the central region of the presumed transmembrane domain remains helical for the entire duration of the simulation. For the SKP peptide, again, residues 4−16 remain helical for most of the simulation, but, as was observed in the other three simulations in POPC bilayers, near the end of the simulation, the transmembrane domain remained helical but with fraying observed at the ends of the peptide. For the SA peptide, the kink that was introduced near the 17th residue to orient the non-transmembrane domain parallel to the lipid−water interface, seems to induce a non-helical structure in the non-transmembrane domain, as also seen in the experiments.

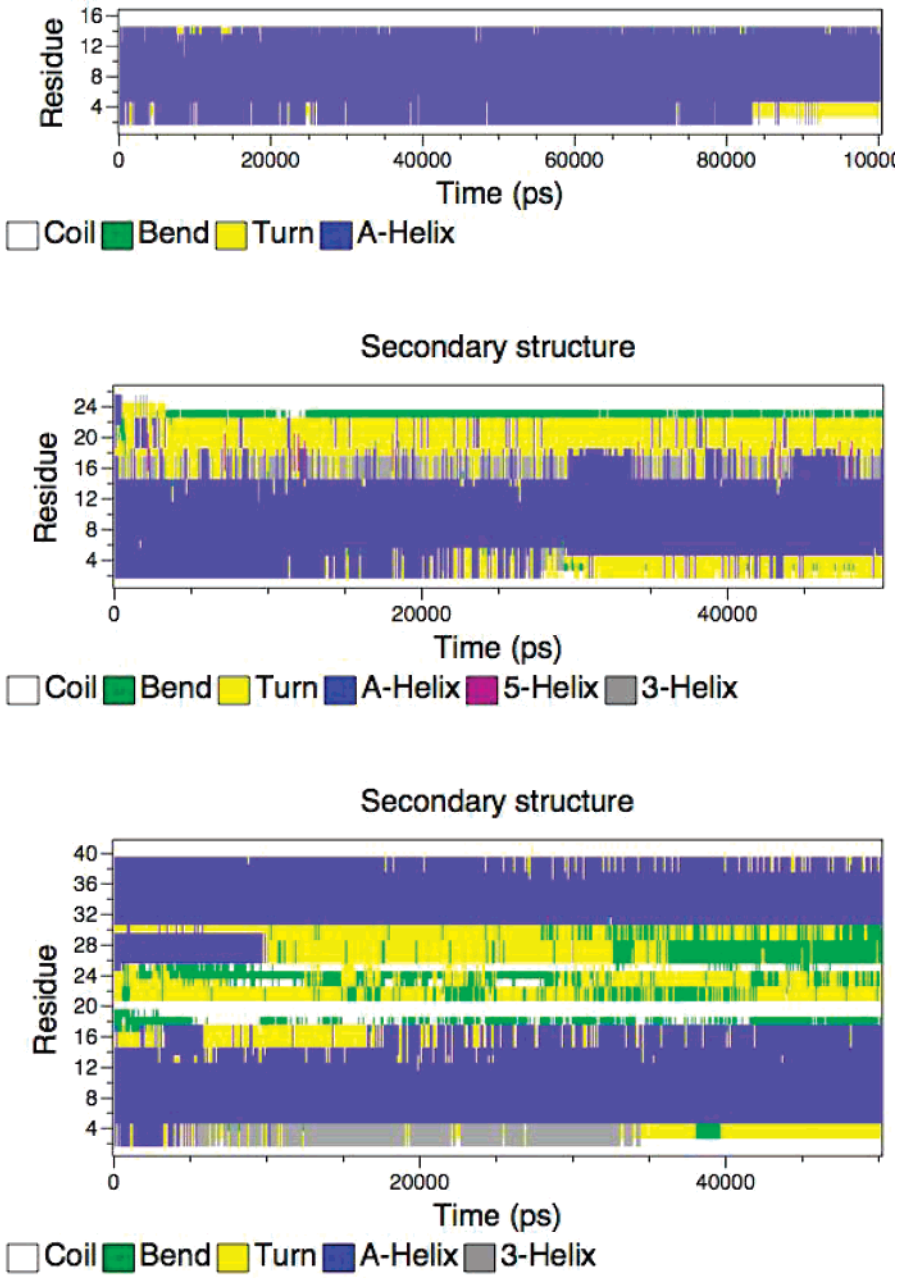

FIGURE 4: Secondary structure profiles of TM (top), SA (middle), and SKP (bottom) peptides in DMPC bilayers obtained from molecular dynamics simulations. Blue color represents α-helical structure.

However, for the SKP peptide, some residual helicity remains in the non-transmembrane domain throughout the simulation. Presumably, longer simulations would enable the non-transmembrane domain to attain its preferred secondary structure, which might well be completely devoid of helicity. Although the final structure of the whole peptide is not completely obtained over the time scales we can obtain, it is clear that in stark contrast to the non-transmembrane domain, the transmembrane domain remains mostly helical in all of the simulations, as observed in experiments. We calculated the mean helicity of the peptides in POPC and DMPC lipid bilayers. The data are presented in Table 1. These simulation results are in good agreement with the CD and MAS experimental results.

Peptide-Induced Disorder in Bilayers. Because a cell-permeable peptide interacts with membranes and could disrupt the lipid bilayer structure to carry out its function, it is important to examine whether SKP and SA induce any changes in the lamellar phase structure of POPC and DMPC bilayers. These results are also essential for interpreting the NMR spectra of mechanically aligned lipid samples in terms of peptide orientation. Therefore, the ^{31}P chemical shift spectra of POPC and DMPC MLVs containing various concentrations (up to 5 mol %) of peptides were obtained at 30 °C. Representative spectra are given in Figure 5. The spectra of all MLV samples (Figure 5A) suggest that the

Table 1: Overall Helicity of Peptides in Phospholipid Bilayers Measured from Molecular Dynamics Simulations and Circular Dichroism Experiments

method		SA	SKP	TM
simulations:	POPC	61%	42%	78%
	DMPC	57%	49%	83%
experiments		60%	45%	not determined

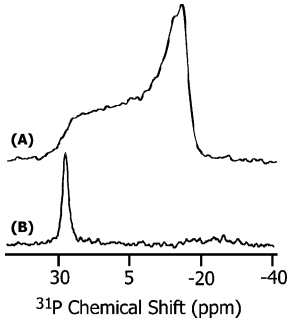

FIGURE 5: ^{31}P chemical shift spectra of (A) multilamellar vesicles and (B) mechanically aligned POPC bilayers containing 3 mol % SKP peptide at 30 °C. About 1500 and 150 scans were used to obtain spectra A and B, respectively.

bilayers were in the lamellar phase. However, the observation of a single narrow peak near the low-field edge of an unoriented spectrum (∼30 ppm) (Figure 5B) suggests that the lipid bilayers were well-hydrated and well-aligned in glass plate samples. These spectra indicate that the interaction of peptides with lipids do not significantly disrupt the lamellar phase bilayer structure of the samples under study. In addition, the ^{31}P data from POPC and DMPC bilayers suggest that the hydrophobic mismatch between the hydrophobic thickness of the lipid bilayer and the hydrophobic length of the peptide had no significant effect on bilayer structure. Small changes observed in the frequency position of the ^{31}P peak in the aligned spectrum and the span of CSA of MLVs with increasing concentration of the peptide can be attributed to the interaction of the peptide, particularly the charged nuclear localization sequence, with the head group region of lipids. Molecular dynamics simulations confirm these experimental results. We calculated the bilayer thickness in the immediate vicinity of the peptide in all six simulations and compared it to the thickness of bilayers free from the peptide. This approach has been used to calculate peptide-induced bilayer disorder in earlier studies (*56*). We found that bilayer disruption was minimal, with a small (∼1 Å) difference between bilayer widths close to and far away from the peptide.

Orientation of SKP and SA Peptides in Bilayers

Solid-State NMR Experiments. The orientations of SKP and SA in phospholipid bilayers were determined using solid-state NMR experiments on mechanically aligned bilayers containing peptides labeled with ^{15}N at a single site. All aligned ^{15}N chemical shift spectra were interpreted with reference to a powder pattern spectrum obtained from MLVs. A spectrum of MLVs containing 3 mol % SKP peptide labeled with ^{15}N-Leu-11 is given in Figure 6. All aligned ^{15}N spectra showed a single narrow peak suggesting that the embedded peptides have a unique orientation in bilayers; some representative spectra are given in Figures 7 and 8. The measured chemical shift values and the line widths are given in Table 2. These spectra contain a single peak (Figures 7 and 8) in a frequency region close to the parallel edge (∼160−215 ppm) of an unaligned ^{15}N chemical shift anisotropy (*57*) spectrum (Figure 6). Because most of the ^{15}N-labeled residues are most likely located in the hydrophobic regions of the bilayer, providing considerably less conformational or dynamic disorder, narrow lines are observed in the spectra of aligned samples. However, some

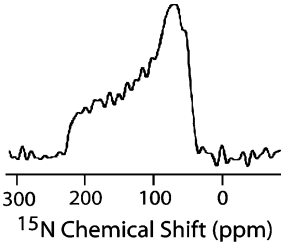

FIGURE 6: ^{15}N chemical shift spectrum of POPC multilamellar vesicles containing 3 mol % ^{15}N-Leu$_{11}$ SKP at −10 °C. A 1 ms cross-polarization time, 4000 scans, and a recycle delay of 3 s were used; all other experimental conditions were as mentioned in the text. The principal components of the amide-^{15}N chemical shift tensor, directly measured from the powder pattern spectrum, are 51 ± 2, 72 ± 2, and 225 ± 2 ppm.

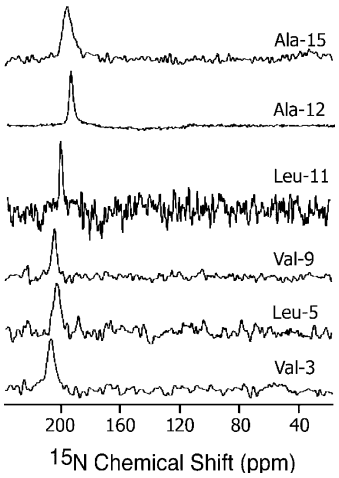

FIGURE 7: ^{15}N chemical shift spectra of mechanically aligned POPC bilayers containing 3 mol % SKP peptides labeled with the ^{15}N isotope at 30 °C. About 600, 400, 800, 400, 4000, and 2000 scans were used to obtain the spectra of peptides labeled with ^{15}N at the amide site Val-3, Leu-5, Val-9, Leu-11, Ala-12, and Ala-15 residues respectively. Other experimental details are given in the text.

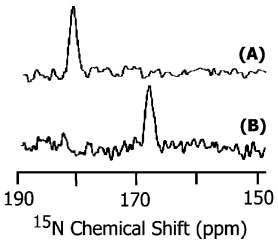

FIGURE 8: ^{15}N chemical shift spectra of mechanically aligned DMPC bilayers containing 3 mol % of (A) SA and (B) SKP peptides labeled with the ^{15}N isotope at the amide site of Leu-11. About 4000 scans were used to obtain the spectra. Other experimental details are as given in the text.

amphipathic peptides oriented near the surface of bilayers could result in broad lines due to heterogeneous orientation (*12*, *15*, *58*) or narrow lines due to motion (*59*). The observed line widths range from 1.8 to 6 ppm and did not depend on the RF power of proton decoupling. The largest line width observed for the Ala-15 residue could be attributed to the conformational heterogeneity of this residue because it is near a Pro residue, which is at a junction of the hydrophobic and hydrophilic regions of the peptide. The chemical shift values measured from SKP and SA are, within experimental errors, similar in POPC bilayers, whereas they are different in DMPC bilayers (Table 2). Because the peptide forms a helical structure in lipid bilayers, these data can be interpreted

Table 2: Experimentally Measured ^{15}N Chemical Shift (Figure 4) and $^{1}H-^{15}N$ Dipolar Coupling (Figure 5) Values of SKP and SA Peptides Embedded in Mechanically Aligned POPC and DMPC Lipid Bilayers at 30 °C

peptide	V_3	L_5	V_9	L_{11}	A_{12}	A_{15}
			POPC (SKP or SA)			
chemical shift (ppm)	210 ± 2	203 ± 3	205 ± 1.5	200 ± 0.9	195 ± 1	198 ± 3
dipolar coupling (kHz)[a]	9.5	7.2	7.0	9.3	7.7	8.2
			SKP in DMPC			
chemical shift (ppm)	190 ± 2	172 ± 1.7	178 ± 2	167 ± 1	170 ± 1	168 ± 2
dipolar coupling (kHz)[a]	8.5	3.5	3.0	8.0	5.0	7.0
			SA in DMPC			
chemical shift (ppm)	200 ± 2	185 ± 1	192 ± 1	181 ± 1.4	180 ± 1	178 ± 2
dipolar coupling (kHz)[a]	9.0	5.0	4.8	9.0	5.5	8.5

[a] On the basis of line widths, the errors in the reported dipolar couplings are estimated to be about ±0.3 to ±0.4 kHz.

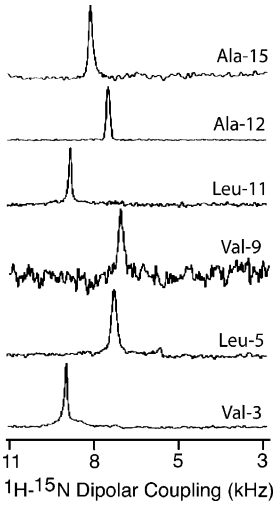

FIGURE 9: $^{1}H-^{15}N$ dipolar coupling spectra of aligned POPC bilayers containing 3 mol % SKP peptides. Because a dipolar coupling spectrum is symmetric with respect to zero frequency, half of each spectrum is presented. These spectra were extracted from 2D PISEMA spectra (not shown). The 2D PISEMA spectra were obtained using a 0.75 ms cross-polarization time, 48 t_1 experiments, 800 scans, and a recycle delay of 3 s.

Table 3: Average Tilt Angles from Experiments and Molecular Dynamics Simulations of Lipid Bilayers Containing SA, SKP, or TM Peptides

tilt angle	SA (50ns)	SKP (50ns)	TM (100ns)
	DMPC bilayers		
simulations	22.3 ± 6.3°	31.7 ± 8.3°	24.6 ± 4.6°
experimental	25 ± 3°	30 ± 3°	
	POPC bilayers		
simulations	13.3 ± 6.7°	16.4 ± 4.0°	19.8 ± 1.0°
experimental	15 ± 3°	15 ± 3°	

in terms of the orientation of the peptide in bilayers. On the basis of the reported structural studies on the membrane-associated peptides using solid-state NMR (*14*, *18*, *40*), these data reveal the transmembrane orientation of the helical region of these peptides.

A 2D PISEMA (*38*−*40*) experiment that correlates the ^{15}N chemical shift and $^{1}H-^{15}N$ dipolar coupling was performed on mechanically aligned bilayer samples. $^{1}H-^{15}N$ dipolar coupling spectra extracted from the 2D PISEMA spectra of different samples are given in Figures 9 and 10. As demonstrated in previous studies, PISEMA provides narrow lines by suppressing $^{1}H-^{1}H$ dipolar interactions (*38*−*40*). Observed line widths range from 0.3 to 0.6 kHz. Because

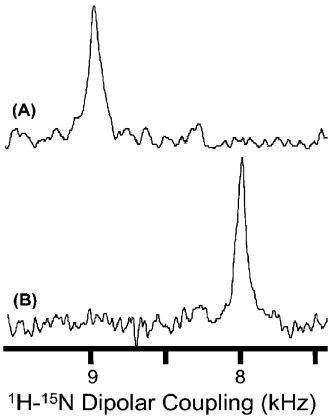

FIGURE 10: $^{1}H-^{15}N$ dipolar coupling spectra of aligned DMPC bilayers containing 3 mol % of (A) SA and (B) SKP peptides labeled with the ^{15}N isotope at the amide site of Leu_{11}. The 2D PISEMA spectra were obtained using a 0.75 ms cross-polarization time, 64 t_1 experiments, 640 scans, and a recycle delay of 3 s.

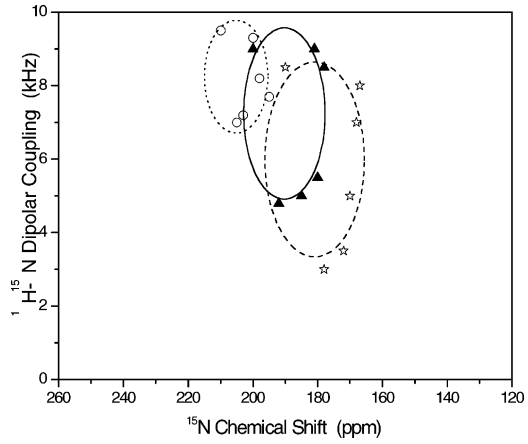

FIGURE 11: Experimental (data points) and simulated (dotted, dashed, or solid lines) PISA wheels corresponding to the hydrophobic transmembrane regions of peptides SKP or SA in POPC ((○) and (....)), SA in DMPC ((▲) and (—)) and SKP in DMPC (stars and (---)) bilayers. Experimental points are generated from the data given in Table 2.

each sample consisted of a single-site ^{15}N-labeled peptide, an off-resonance dependence of the PISEMA sequence (*40*) was minimized by setting ^{1}H and ^{15}N carrier frequencies close to the amide-^{1}H and -^{15}N resonances, respectively. Therefore, errors in the measured parameters due to the variation of the scaling factor of the sequence were minimized.

PISA (polarity index slant angle) wheels (*60*, *61*) generated from PISEMA spectra of ^{15}N chemical shifts and $^{1}H-^{15}N$

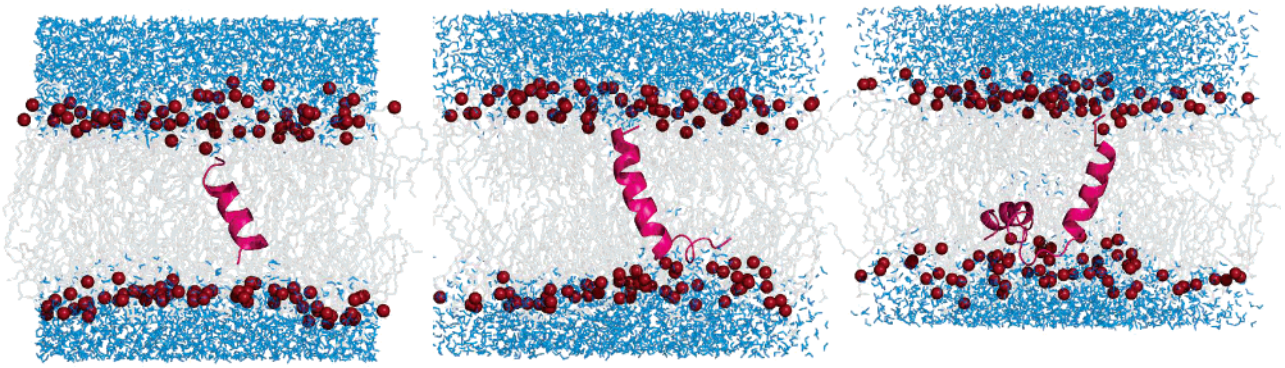

FIGURE 12: Snapshots at the end of molecular dynamics simulations for TM (left), SA (middle), and SKP (right) peptides in DMPC bilayers. The lipid tails are shown in gray, the water molecules in blue, and the lipid phosphorus atoms in red. The peptide is shown as pink ribbons.

dipolar couplings of mechanically aligned samples are given in Figure 11, along with simulated PISA wheel spectra. The simulations were carried out using the SIMMOL program (*62*, *63*). Even though there are not enough experimental points to define the complete shape of the PISA wheel, the simulated and experimental spectra are in good agreement. A comparison of the simulated and experimental results suggests that the helical domain is transmembrane but tilted away from the bilayer normal. The tilt angles are given in Table 3. Interestingly, the tilt angles measured in POPC are smaller but are different in DMPC bilayers. Errors on the reported tilt angles are estimated from the line widths observed in the chemical shift and dipolar coupling spectra. However, there could be additional contributions to the error from the variation of chemical shift tensors (*57*, *64*) from the model tensor used for these calculations and because of peptide dynamics that would have influenced the observed experimental parameters. Nevertheless, the reported tilt angles are in good agreement with results obtained from MD simulations discussed below.

Molecular Dynamics Simulations. We observed the tilting of peptides away from their original vertical transmembrane orientation in all six simulations. In Figure 12, we show snapshots at the end of three simulations (TM, SA, and SKP in DMPC bilayers). It is clear that the non-transmembrane domain of the SA peptide is fully frayed, with no residual helicity. Residues 30 to 38 of the SKP peptide retain their initial helicity, whereas residues 18 to 30 seem to lose their helicity quickly. However, the region of residual helicity is far away from the transmembrane domain and presumably will not affect the tilt behavior of the transmembrane region. We calculated the tilt angle of the transmembrane segment relative to the bilayer normal for all six simulations. The helical axis was defined by selecting two points at the top and bottom of the transmembrane segment. The top point was chosen to be the center of mass of the backbone atoms of residues 3, 4, and 5, whereas the bottom point was chosen to be the center of mass of the backbone atoms of residues 12, 13, and 14. In Figure 13, we show the tilt angle as a function of time for a representative simulation (TM peptide in POPC bilayers). The average tilt angle was calculated for all simulations and is presented in Table 3. The first 20 ns of each simulation was taken to be an equilibration period and was not used to calculate the average. The standard error was estimated by a block-averaging procedure. The peptides show a consistently larger tilt in DMPC bilayers than in the POPC bilayers, which is expected because POPC bilayers have a larger hydrophobic width than DMPC bilayers, and therefore, the disparity between the hydrophobic length of the peptide and the hydrophobic width is greater for DMPC. It should be noted that the standard errors of tilt angles are rather large, especially for SA and SKP peptides. This is due to the large timescales required for the equilibration of peptide tilt in phospholipid bilayers. In a recent simulation study (*56*), we found that even 100 ns may not be sufficient to fully equilibrate peptide tilt in lipid bilayers. Thus, longer simulations will be required to provide a quantitatively more accurate tilt angle. Nevertheless, qualitatively, the peptides show a consistently larger tilt in DMPC bilayers than in POPC bilayers, in agreement with experimental results.

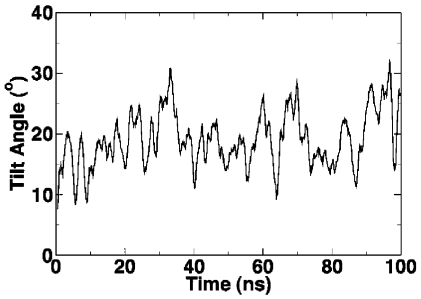

FIGURE 13: Tilt angle as a function of simulation time for a representative simulation for the TM peptide in POPC bilayers. The tilt angle is shown as a running average.

DISCUSSION

Cell-signaling peptides, such as SA and SKP, have been used to carry functional nuclear localization sequences across the cell membrane (*6*, *8*, *9*). Previous studies have shown that these peptides are efficient in transporting nuclear localization sequences for intracellular activities (*1*−*10*). However, the mechanism of the transport activity and interaction of these peptides with membranes are not clear. In this study, solid-state NMR experiments and molecular dynamics simulations were used to investigate the interaction of SA and SKP peptides with model membranes. In particular, the structure and folding of the hydrophobic domain of these peptides in membrane bilayers were determined, and the effect of peptide−membrane interactions on lipid bilayer structure was also examined. The effect of hydrophobic mismatch between the hydrophobic length of

the peptide and the thickness of lipid bilayers on the folding of the peptide was investigated using thicker (POPC) and thinner (DMPC) bilayers.

Secondary Structure. Results obtained from CD experiments on SUVs (Figure 2) and solution NMR experiments on detergent micelles (data not given) suggest that the main conformation of both of the peptides is helical in membrane environments. CD results suggested that SA (~60%) is more helical than SKP (~45%), which is in agreement with the qualitative structure prediction analysis. The difference in the helical content could be due to the difference in the hydrophilic nuclear localization sequences of these peptides. The non-helical NLS of SKP (25 residues) is longer than that of SA (7 residues), and hence, its contribution to the non-helicity of the peptide is greater. In addition, the hydrophobic spacer region containing three Ala residues in SA could increase the helicity of the peptide by better insulating the non-helical region from the helical transmembrane domain. The CD results are further confirmed using REDOR experiments on MLVs containing peptides labeled with $^{13}C'$ and ^{15}N isotopes (Figure 3). The observation of similar $^{13}C'$ chemical shift values from DMPC and POPC bilayers suggests that the conformation is independent of the thickness of the bilayer.

Topology and Tilt of Peptides in Membrane Bilayers. PISA wheels (Figure 11) generated from the experimentally measured chemical shift (Figures 7 and 8) and dipolar coupling (Figures 9 and 10) values (Table 2) on mechanically aligned bilayers containing peptides suggest that the hydrophobic domain (residues 1 to 15 in Figure 1) of both of the peptides has a transmembrane orientation in DMPC and POPC bilayers. However, the helical axis of this domain is tilted away from the direction of the bilayer normal in both types of bilayers with a larger tilt in thinner DMPC bilayers than in thicker POPC bilayers. These results are in very good agreement with molecular dynamics simulations. Experimental results suggest that the helical axis of both peptides is tilted 15 ± 3° relative to the normal in POPC bilayers compared to the MD predicted tilts of 13.3° for SA and 16.4° for SKP. In DMPC bilayers, SA has an experimentally determined tilt of 25 ± 3°, whereas for SKP, it is 30 ± 3° compared to predicted values of 22.3° and 31.7°, respectively. The trends and even the magnitudes of the tilts in the simulations are remarkably consistent with experimental values. The simulations on the hydrophobic sequence (the TM peptide) alone suggest that the tilt angle is 19.8° and 24.6° in POPC and DMPC bilayers, respectively.

Solid-state NMR experiments have been successfully used to understand the topology of several membrane-associated peptides and proteins (*13*, *18*−*21*, *40*, *60*, *61*). Particularly, the high resolution rendered by 2D PISEMA experiments has yielded PISA wheel patterns of membrane-bound helices (*13*, *18*, *40*, *60*, *61*). Images of proteins and peptides have been used to address various biological questions related to membrane−peptide and peptide−peptide interactions that determine the function of membrane-associated proteins (*11*, *40*, *65*). Our PISEMA results presented in this article are consistent with the interpretations and explanations provided by previous studies on different transmembrane helical systems (*13*, *18*, *40*, *60*, *61*, *65*). Interestingly, the tilt angles measured from solid-state NMR experiments are also in good agreement with MD simulations. More generally, our results and those of others indicate that a combination of MD simulations and solid-state NMR structural constraints could be a practical way to solve some of the challenging problems involved in studying membranes and membrane−peptide interactions. For example, MD simulations have yielded a unique structure of gramicidin when combined with solid-state NMR structural constraints obtained from mechanically aligned bilayers (*66*). In addition, a recent study combining MD simulations with NMR determined the orientation and conformational preference of leucine−enkephalin in DMPC bilayers (*67*). Similar studies are increasingly being carried out in several laboratories. Therefore, we believe that although both NMR and MD simulations will continue to be developed, a suitable combination of the two can provide insights into the structure, dynamics, folding, oligomerization, topology, and function of some of the most challenging membrane-associated peptides and proteins.

Effect of Hydrophobic Mismatch. Recent studies have shown that the hydrophobic mismatch between the hydrophobic length of a helical peptide and the hydrophobic thickness of the lipid bilayer can significantly affect the backbone conformation, membrane orientation, tilt (the angle between the helical axis and the bilayer normal), and oligomerization of the peptide (*65*, *68*−*78*). It could also lead to changes in the phase, order/disorder, and curvature of lipid bilayers (*68*). Although most previous studies utilized designed peptides (*68*, *70*−*72*, *74*−*76*), in this study, we considered the effect of hydrophobic mismatch on the folding and tilt of functional peptides. ^{31}P NMR and MD simulation results suggest that the hydrophobic mismatch, in both SA and SKP peptides, did not alter the phase, structure, and order of lipid bilayers. CD and REDOR experiments and MD simulations showed that the backbone conformation of SA and SKP peptides is independent of the thickness of the bilayer, suggesting that the hydrophobic mismatch does not affect the structure of the peptides either. However, as mentioned above, ^{15}N NMR and MD simulations results reveal that rather than altering either the membrane or the peptide structure, hydrophobic mismatch is accommodated through tilting of the peptides to keep their hydrophobic domain within the hydrophobic region of the bilayer. The measured and simulated tilt angles for SA and especially SKP are generally larger than those observed for model peptides such as KALP peptides (*68*). However, the observed qualitative dependence of the tilt of SA and SKP peptides on the bilayer thickness of DMPC and POPC is consistent with recent NMR studies on other transmembrane peptide fragments (*65*, *78*). For example, Cross and co-workers used NMR spectra of aligned bilayers containing the tetrameric M2 protein of influenza A in DLPC, DMPC, and POPC bilayers to understand the effect of hydrophobic mismatch on the tilt of the helical transmembrane domain of the protein (*69*, *78*). Recently, Opella and co-workers used PISA wheels to determine the effect of hydrophobic mismatch on the tilt of a 36-residue N-terminal channel-forming segment of Vpu protein from HIV (*65*). Interestingly, they reported a large tilt angle of 51° and a helix kink in lipid bilayers (*65*). Therefore, in the absence of oligomerization and disorder in the structure of lipids, a large tilt angle is possible for membrane-associated proteins/peptides, whereas the extent of the tilt depends on the length of the hydrophobic sequence and membrane composition (*65*, *69*, *77*, *78*). The tilted

transmembrane orientation of SA and SKP peptides and their avoidance of the disruption of cell membrane integrity could be responsible for their efficient transport of nuclear localization sequences across the plasma membrane.

REFERENCES

1. Zorko, M., and Langel, U. (2005) Cell-penetrating peptides: mechanism and kinetics of cargo delivery, *Adv. Drug Delivery Rev. 57*, 529−545.
2. Boon, J. M., and Smith B. D. (2002) Synthetic membrane transporters, *Curr. Opin. Chem. Biol. 6*, 749−756.
3. Hawiger, J. (1999) Noninvasive intracellular delivery of functional peptides and proteins, *Curr. Opin. Chem. Biol. 3*, 89−94.
4. Thoren, P. E., Persson, D., Esbjorner, E. K., Goksor, M., Lincoln, P., and Norden, B. (2004) Membrane binding and translocation of cell-penetrating peptides, *Biochemistry 43*, 3471−3489.
5. Veach, R. A., Liu, D., Yao, S., Chen, Y., Liu, X. Y., Downs, S., and Hawiger, J. (2004) Receptor/transporter-independent targeting of functional peptides across the plasma membrane, *J. Biol. Chem. 279*, 11425−11431.
6. Lin, Y. Z., Yao, S. Y., Veach, R. A., Torgerson, T. R., and Hawiger, J. (1995) Inhibition of nuclear translocation of transcription factor NF-kappa B by a synthetic peptide containing a cell membrane-permeable motif and nuclear localization sequence, *J. Biol. Chem. 270*, 14255−14258.
7. Christiaens, B., Grooten, J., Reusens, M., Joliot, A., Goethals, M., Vandekerckhove, J., Prochiantz, A., and Rosseneu, M. (2004) Membrane interaction and cellular internalization of penetratin peptides, *Eur. J. Biochem. 271*, 1187−1197.
8. Lin, Y. Z., Tao, S. Y., and Hawiger, J. (1996) Role of the nuclear localization sequence in fibroblast growth factor-1-stimulated mitogenic pathways, *J. Biol. Chem. 271*, 5305−5308.
9. Rojas, M., Yao, S. Y., and Lin, Y. Z. (1996) Controlling epidermal growth factor (EFG)-stimulated Ras activation in intact cells by a cell-permeable peptide mimicking phosphorylated EGF receptor, *J. Biol. Chem. 271*, 27456−27461.
10. Liu, X. Y., Timmons, S., Lin, Y. Z., and Hawiger, J. (1996) Identification of a functionally important sequence in the cytoplasmic tail of integrin b3 by using cell-permeable peptide analog, *Proc. Natl. Acad. Sci. U.S.A. 93*, 11819−11824.
11. Hu, J., Fu, R., Nishimura, K., Zhang, L., Zhou, H. X., Busath, D. D., Vijayvergiya, V., and Cross, T. A. (2006) Histidines, heart of the hydrogen ion channel from influenza A virus: Toward an understanding of conductance and proton selectivity, *Proc. Natl. Acad. Sci. U.S.A. 103*, 6865−6870.
12. Henzler-Wildman, K. A., Lee, D. K., and Ramamoorthy, A. (2003) Mechanism of lipid bilayer disruption by the human antimicrobial peptide, LL-37, *Biochemistry 42*, 6545−6558.
13. Marassi, F. M. (2001) A simple approach to membrane protein secondary structure and topology based on NMR spectroscopy, *Biophys. J. 80*, 994−1003.
14. Strandberg, E., Wadhwani, P., Tremouilhac, O., Durr, U. H. N., and Ulrich, A. S. (2006) Solid-state NMR analysis of the PGLa peptide orientation in DMPC bilayers: Structural fidelity of H-2-labels versus high sensitivity of F-19-NMR, *Biophys. J. 90*, 1676−1686.
15. Hallock, K. J., Lee, D. K., and Ramamoorthy, A. (2003) MSI-78, an analogue of the magainin antimicrobial peptides, disrupts lipid bilayer structure via positive curvature strain, *Biophys. J. 84*, 3052.
16. Yang, J., Prorok, M., Castellino, F. J., and Weliky, D. P. (2004) Oligomeric beta-structure of the membrane-bound HIV-1 fusion peptide formed from soluble monomers, *Biophys. J. 87*, 1951−1963.
17. Lu, J. X., Damodaran, K., Blazyk, J., and Lorigan, G. A. (2005) Solid-state nuclear magnetic resonance relaxation studies of the interaction mechanism of antimicrobial peptides with phospholipid bilayer membranes, *Biochemistry 44*, 10208−10217.
18. Opella, S. J., and Marassi, F. M. (2004) Structure determination of membrane proteins by NMR spectroscopy, *Chem. Rev. 104*, 3587−3606.
19. Tian, C. L., Gao, P. F., Pinto, L. H., Lamb, R. A., and Cross, T. A. (2004) Initial structural and dynamic characterization of the M2 protein transmembrane and amphipathic helices in lipid bilayers, *Protein Sci. 12*, 2597−2605.
20. Quine, J. R., and Cross, T. A. (2000) Protein structure in anisotropic environments: Unique structural fold from orientational constraints, *Concepts Magn. Reson. 12*, 71−82.
21. Gong, X. M., Choi, J. Y., Franzin, C. M., Zhai, D. Y., Reed, J. C., and Marassi, F. M. (2004) Conformation of membrane-associated proapoptotic tBid, *J. Biol. Chem. 279*, 28954−28960.
22. Porcelli, F., Buck-Koehntop, B., Thennarasu, S., Ramamoorthy, A., and Veglia, G. (2006) Structures of the dimeric and monomeric variants of magainin antimicrobial peptides (MSI-78 and MSI-594) in micelles and bilayers by NMR spectroscopy, *Biochemistry 45*, 5793−5799.
23. McDowell, L. M., and Schaefer, J. (1996) High-resolution NMR of biological solids, *Curr. Opin. Struct. Biol. 6*, 624−629.
24. Kamihira, M., Vosegaard, T., Mason, A. J., Straus, S. K., Nielsen, N. C., and Watts, A. (2005) Structural and orientational constraints of bacteriorhodopsin in purple membranes determined by oriented-sample solid-state NMR spectroscopy, *J. Struct. Biol. 149*, 7−16.
25. Crocker, E., Eilers, M., Ahuja, S., Hornak, V., Hirshfeld, A., Sheves, M., and Smith, S. O. (2006) Location of Trp265 in metarhodopsin II: implications for the activation mechanism of the visual receptor rhodopsin, *J. Mol. Biol. 357*, 163−172.
26. Sharpe, S., Yau, W. M., and Tycko, R. (2006) Structure and dynamics of the HIV-1 Vpu transmembrane domain revealed by solid-state NMR with magic-angle spinning, *Biochemistry 45*, 918−933.
27. Thonpson, L. K. (2002) Solid-state NMR studies of the structure and mechanisms of proteins, *Curr. Opin. Struct. Biol. 12*, 661−669.
28. Lange, A., Giller, K., Hornig, S., Martin-Eauclaire, M. F., Pongs, O., Becker, S., and Baldus, M. (2006) Toxin-induced conformational changes in a potassium channel revealed by solid-state NMR, *Nature 440*, 959−962.
29. Andronesi, O. C., Becker, S., Seidel, K., Heise, H., Young, H. S., and Baldus, M. (2005) Determination of membrane protein structure and dynamics by magic-angle-spinning solid-state NMR spectroscopy, *J. Am. Chem. Soc. 127*, 12965−12974.
30. Baldus, M. (2006) Spectral Assignment of (Membrane) Proteins under Magic-Angle Spinning, in *NMR Spectroscopy of Biological Solids* (Ramamoorthy, A., Ed.) pp 39−56, Taylor and Francis, New York.
31. Todokoro, Y., Yumen, I., Fukushima, K., Kang, S. W., Park, J. S., Kohno, T., Wakamatsu, K., Akutsu, H., and Fujiwara, T. (2006) Structure of tightly membrane-bound mastoparan-X, a G-protein-activating peptide, determined by solid-state NMR, *Biophys. J. 91*, 1368−1379.
32. Luca, S., Heise, H., and Baldus, M. (2003) High-resolution solid-state NMR applied to polypeptides and membrane proteins, *Acc. Chem. Res. 36*, 858−865.
33. Porcelli, F., Buck, B., Lee, D. K., Hallock, K. J., Ramamoorthy, A., and Veglia, G. (2004) Structure and orientation of pardaxin determined by NMR experiments in model membranes, *J. Biol. Chem. 279*, 46815−46823.
34. Tieleman, D. P., Berendsen, H. J. C., and Sansom, M. S. P. (1999) Surface binding of alamethicin stabilizes its helical structure: molecular dynamics simulations, *Biophys. J. 76*, 3186 −3191.
35. Kandasamy, S. K., and Larson, R. G. (2004) Binding and insertion of alpha- helical anti-microbial peptides in POPC bilayers studied by molecular dynamics simulations, *Chem. Phys. Lipids 132*, 113−132.
36. Lensink, M. F., Christiaens, B., Vandekerckhove, J., Prochiantz, A., and Rosseneu, M. (2005) Penetratin-membrane association: W48/R52/W56 shield the peptide from the aqueous phase, *Biophys. J. 88*, 939−952.
37. Gullion, T., and Schaefer, J. (1987) Rotational-echo double-resonance NMR, *J. Magn. Reson. 81*, 196−200.
38. Wu, C. H., Ramamoorthy, A., and Opella, S. J. (1994) High Resolution Heteronuclear Dipolar Solid-state NMR spectroscopy, *J. Magn. Reson., Ser. A 109*, 270.
39. Ramamoorthy, A., Wu, C. H., and Opella, S. J. (1999) Experimental aspects of multidimensional solid-state NMR correlation spectroscopy, *J. Magn. Reson. 140*, 131.
40. Ramamoorthy, A., Wei, Y., and Lee, D. K. (2004) PISEMA solid-state NMR spectroscopy, *Annu. Rep. NMR Spectrosc. 52*, 1−52.

41. Hallock, K. J., Henzler Wildman, K. A., Lee, D. K., and Ramamoorthy, A. (2002) Sublimable solids can be used to mechanically align lipid bilayers for solid-state NMR studies, *Biophys. J. 82*, 2499.

42. Washburn, E., West, C. J., and Hull, C. (1926) *International Critical, Tables of Numerical Data, Physics, Chemistry, and Technology*, McGraw-Hill, New York.

43. Pines, A., Gibby, M. G., and Waugh, J. (1973) Proton-enhanced NMR of dilute spins in solids, *J. Chem. Phys. 59*, 569−590.

44. Bennet, A. E., Rienstra, C. M., Auger, M., Lakshmi, K. V., and Griffin, R. G. (1995) Heteronuclear decoupling in rotating solids, *J. Chem. Phys. 103*, 6951−6958.

45. Metz, G., Wu, X., and Smith, S. O. (1994) Ramped-amplitude cross polarization in magic-angle-spinning NMR, *J. Magn. Reson., Ser. A 110*, 219−227.

46. Lee, M., and Goldburg, W. I. (1965) Nuclear-magnetic-resonance line narrowing by a rotating Rf field, *Phys. Rev. 140*, 1261.

47. Yang, J., Parkanzky, P. D., Bodner, M. L., Duskin, C. A., and Weliky, D. P. (2002) Application of REDOR subtraction for filtered MAS observation of labeled backbone carbons of membrane-bound fusion peptides, *J. Magn. Reson. 159*, 101−110.

48. Lindahl, E., Hess, B., and van der Spoel., D. (2001) GROMACS 3.0: a package for molecular simulation and trajectory analysis, *J. Mol. Model. 7*, 306−317.

49. Berger, O., Edholm, O., and Jahnig, F. (1997) Molecular dynamics simulations of a fluid bilayer of dipalmitoylphosphatidylcholine at full hydration, constant pressure, and constant temperature, *Biophys. J. 72*, 2002−2013.

50. Guex, N., and Peitsch, M. C. (1997) SWISS-MODEL and the Swiss- PdbViewer: An environment for comparative protein modeling, *Electrophoresis 18*, 2714−2723.

51. Essmann, U., Perera, L., Berkowitz, M. L., Darden, T., Lee, H., and Pedersen, L. G. (1995) A smooth particle mesh ewald method, *J. Chem. Phys. 103*, 8577−8593.

52. Faraldo-Gomez, J. D., Smith, G. R., and Sansom, M. S. P. (2002) Setting up and optimization of membrane protein simulations, *Eur. Biophys. J. 31*, 217−227.

53. Toke, O., O'Connor, R. D., Weldeghiorghis, T. K., Maloy, W. L., Glaser, R. W., Ulrich, A. S., and Schaefer, J. (2004) Structure of (KIAGKIA)(3) aggregates in phospholipid bilayers by solid-state NMR, *Biophys. J. 87*, 675−687.

54. Wei, Y., Lee, D. K., and Ramamoorthy, A. (2001) Solid-state ^{13}C chemical shift anisotropy tensors of polypeptides, *J. Am. Chem. Soc. 123*, 6118−6126.

55. Tuzi, S., Komoto, T., Ando, I., Saito, H., Shoji, A., and Ozaki, T. (1983) C-13- NMR chemical-shift and conformation of L-alanine residues incorporated into poly(beta-benzyl L-aspartate) in the solid-state, *Biopolymers 26*, 1983−1992.

56. Kandasamy, S. K., and Larson, R. G. (2006) Molecular dynamics simulations of model trans-membrane peptides in lipid bilayers: a systematic investigation of hydrophobic mismatch, *Biophys. J. 90*, 2326−2343.

57. Poon, A., Birn, J., and Ramamoorthy, A. (2004) Variation of amide-^{15}N chemical shift tensors in proteins, *J. Phys. Chem. B 108*, 16577−16585.

58. Ramamoorthy, A., Marassi, F. M., Zasloff, and Opella, S. J. (1995) 3- Dimensional solid-state NMR spectroscopy of a peptide oriented in membrane bilayers, *J. Biomol. NMR 6*, 329−334.

59. Aisenbrey, C., Bechinger, B. (2004) Investigations of polypeptide rotational diffusion in aligned membranes by ^{2}H and ^{15}N solid-State NMR spectroscopy, *J. Am. Chem. Soc. 126*, 16676−16683. Chekmenev, E. Y., Vollmar, B. S., Forseth, K. T., Manion, M. N., Jones, S. M., Wagner, T. J., Endicott, R. M., Kyriss, B. P., Homem, L. M., Pate, M., He, J., Raines, J., Gor'kov, P., Brey, W. W., Mitchell, D. J., Auman, A. J., Ellard-Ivey, M. J., Blazyk, J., Cotton, M. (2006) Investigating molecular recognition and biological function at interfaces using piscidins, antimicrobial peptides from fish, *Biochim. Biophys. Acta 1758*, 1359−1372.

60. Marassi, F. M., and Opella, S. J., (2000) A solid-state NMR index of helical membrane protein structure and topology, *J. Magn. Reson. 144*, 150−155.

61. Wang, J., Denny, J., Tian, C., Kim, S., Mo, Y., Kovacs, F., Song, Z., Nishimura, K., Gan, Z., Fu, R., Quine, J. R., and Cross, T. A. (2000) Imaging membrane protein helical wheels, *J. Magn. Reson. 144*, 162−167.

62. Bak, M., Rasmussen, J. T., and Nielsen, N. C. (2000) SIMPSON: A general simulation program for solid-state NMR spectroscopy, *J. Magn. Reson. 147*, 296−330.

63. Bak, M., Schultz, R., Vosegaad, T., and Nielsen, N. C. (2002) Specification and visualization of anisotropic interaction tensors in polypeptides and numerical simulations in biological solid-state NMR, *J. Magn. Reson. 154*, 28−45.

64. Lee, D. K., Wittebort, R. J., and Ramamoorthy, A. (1998) Characterization of ^{15}N chemical shift and ^{1}H-^{15}N dipolar coupling interactions in a peptide bond of uniaxially oriented and polycrystalline samples by one-dimensional dipolar: chemical shift solid-state NMR spectroscopy, *J. Am. Chem. Soc. 120*, 8868−8874.

65. Park, S. H., and Opella, S. J. (2005) Tilt angle of a trans-membrane helix is determined by hydrophobic mismatch, *J. Mol. Biol. 350*, 310−318.

66. Allen, T. W., Andersen, O. S., and Roux, B. (2003) Structure of gramicidin A in a lipid bilayer environment determined using molecular dynamics simulations and solid-state NMR data, *J. Am. Chem. Soc. 125*, 9868−9877.

67. Chandrasekar, I., van Gunsteren, W. F., Zandomeneghi, G., Williamson, P. T. F., and Meier, B. H. (2005) Orientation and conformational preference of leucine-enkephalin at the surface of a hydrated dimyristoylphosphatidylcholine bilayer: NMR and MD simulation, *J. Am. Chem. Soc. 128*, 159−170.

68. Killian, J. A., and Nyholm, T. K. M. (2006) Peptides in lipid bilayers: the power of simple models, *Curr. Opin. Struct. Biol. 16*, 1−7.

69. Kovacs, F. A., and Cross, T. A. (1997) Transmembrane four-helix bundle of influenza A M2 protein channel: structural implications from helix tilt and orientation, *Biophys. J. 73*, 2511−2517.

70. White, S. H., and Wimley, W. C. (1998) Hydrophobic interactions of peptides with membrane interfaces, *Biochim. Biophys. Acta 1376*, 339−352.

71. Killian, J. A. (1998) Hydrophobic mismatch between proteins and lipids in membranes, *Biochim. Biophys. Acta 1376*, 401−415.

72. Zhang, Y. P., Lewis, R. N., Hodges, R. S., and McElhaney, R. N. (1992) Interaction of a peptide model of a hydrophobic transmembrane alpha-helical segment of a membrane protein with phosphatidylcholine bilayers: differential scanning calorimetric and FTIR spectroscopic studies, *Biochemistry 31*, 11579−11588.

73. de Planque, M. R., Greathouse, D. V., Koeppe, R. E., II, Schafer, H., Marsh, D., and Killian, J. A. (1998) Influence of lipid/peptide hydrophobic mismatch on the thickness of diacylphosphatidylcholine bilayers. A ^{2}H NMR and ESR study using designed transmembrane alpha-helical peptides and gramicidin A, *Biochemistry 37*, 9333−9345.

74. Harzer, U., and Bechinger, B. (2000) Alignment of lysine-anchored membrane peptides under conditions of hydrophobic mismatch: a CD, ^{15}N and ^{31}P solid-state NMR spectroscopy investigation, *Biochemistry 39*, 13106−13114.

75. Weiss, T. M., van der Wel, P. C., Killian, J. A., Koeppe, R. E., and Huang, H. W. (2003) Hydrophobic mismatch between helices and lipid bilayers, *Biophys. J. 84*, 379−385.

76. Strandberg, E., Ozdirekcan, S., Rijkers, D. T. S., val der Wel, C. A., Koepee, R. E., II, Liskamp, R. M. J., and Killian, J. A. (2004) Tilt angles of transmembrane model peptides in oriented and non-orientated lipid bilayers as determined by ^{2}H solid-state NMR, *Biophys. J. 86*, 3709−3721.

77. Duong-ly, K. C., Nanda, V., Degrado, W. F., and Howard, K. P. (2005) The conformation of the pore region of the M2 proton channel depends on lipid bilayer environment, *Protein Sci. 14*, 856−861.

78. Kovacs, F. A., Denny, J. F., Song, Z., Quine, J. R., and Cross, J. A. (2000) Helix tilt of the M2 transmembrane peptide from influenza A virus: An intrinsic property, *J. Mol. Biol. 295*, 117−125.

BI061895G